

Targeting the Cohesive Cluster Phenotype in Chordoma via $\beta 1$ Integrin Increases Ionizing Radiation Efficacy^{1,2}



William L. Harryman^{*}, Jaime M.C. Gard^{*},
Kelvin W. Pond[†], Skyler J. Simpson^{*,‡},
Lucas H. Heppner^{*}, Daniel Hernandez-Cortes[§],
Andrew S. Little[¶], Jennifer M. Eschbacher[¶] and
Anne E. Cress^{*,†}

^{*}University of Arizona Cancer Center, 1515 N. Campbell Ave., Tucson, AZ, 85724; [†]Department of Cellular and Molecular Medicine, The University of Arizona, 1515 N. Campbell Ave., Tucson, AZ, 85724; [‡]Medical Student Research Program, The University of Arizona College of Medicine, 1515 N. Campbell Ave., Tucson, AZ, 85724; [§]Cancer Biology Research Program, The University of Arizona, 1515 N. Campbell Ave., Tucson, AZ, 85724; [¶]Barrow Neurological Institute, 350 W. Thomas Rd., Phoenix, AZ, 85013

Abstract

Chordoma is a rare, radiation-resistant, skull-base and spinal tumor with high local recurrence containing mixed cell-adhesion phenotypes. We characterized DNA damage response (DDR) signaling (γ H2AX, pKAP1, pATM) and survival response to ionizing radiation (IR) in human chordoma samples (42 resections, 23 patients) to test if blocking cell adhesion sensitizes U-CH1 tumor cells to IR. U-CH1 cells expressed brachyury, YAP, and laminin adhesion receptors (CD49c, CD49f, CD44), and approximately 15% to 20% of U-CH1 cells featured an $\alpha 6$ integrin-dependent (CD49f) cohesive cluster phenotype, which confers therapeutic resistance and aids metastasis. DDR to IR in U-CH1 cells was compared to normal prostate epithelial (PrEC) and tumor cells (DU145). Flow cytometry showed a dose- and time-dependent increase in γ H2AX and pKAP1 expression in all cell lines. However, nearly 50% of U-CH1 cells exhibited nonresponsive phenotype to IR (measured by γ H2AX and pKAP1) independent of cell cycle status. Immunofluorescence microscopy verified that only 15% of U-CH1 clustered cells were γ H2AX or pKAP1 positive (versus 80% of nonclustered cells) 2 hours following 2-Gy IR. Conversely, both tumor cell lines were uniformly defective in pATM response. HYD1, a synthetic ECM ligand, inhibited DDR through an unresolved γ H2AX response. $\beta 1$ integrin-blocking antibody (A11B2) decreased cell survival 50% itself and approximately doubled the IR-induced cell kill at all IR doses observed at 2 and 4 weeks posttreatment. These results suggest that a heterogeneity of DDR to IR exists within a chordoma population. Blocking integrin function alone and/or as an adjuvant to IR may eradicate chordomas containing the cohesive cluster phenotype.

Neoplasia (2017) 19, 919–927

Introduction

Chordoma is a rare cancer accounting for 1% to 4% of all bone malignancies [1,2]. Chordoma histologically suggests a low-grade neoplasm [1]. However, while chordomas are slow growing and radioresistant, they are locally aggressive, invasive, and highly recurrent and present a clinical progression representative of malignant tumors. Chordomas arise from undifferentiated remnants of the primitive notochord [1,3] and surprisingly express

Address all correspondence to: Anne E. Cress, The University of Arizona Cancer Center, Department of Cellular and Molecular Medicine, 1515 N. Campbell Ave., Tucson, AZ 85724, United States.

E-mail: cress@email.arizona.edu

¹Financial support: The research was supported in part by the National Institutes Health: P30CA23074, RO1CA159406, T32CA09213, and T35HL007479.

²The authors declare no conflicts of interest.

Received 30 April 2017; Revised 5 August 2017; Accepted 14 August 2017

© 2017 The Authors. Published by Elsevier Inc. on behalf of Neoplasia Press, Inc. This is an open access article under the CC BY-NC-ND license (<http://creativecommons.org/licenses/by-nc-nd/4.0/>). 1476-5586

<https://doi.org/10.1016/j.neo.2017.08.005>

epithelial-type characteristics [4] and a low growth fraction, indicative of slow-growing disease. Chordomas impinge on critical nerve functions present within the clival, vertebral, and sacral regions of the spine [5] and can locally invade surrounding laminin-rich muscle. Originally thought to occur predominantly in the sacrum, chordomas are equally distributed between three primary locations: 29.2% in the sacrum, 32% in the skull base (clival), and 32.8% in the mobile spine (cervical, thoracic, and lumbar) [6]—however, other research has suggested 50% sacral, 35% clival, and 15% mobile spine [5]. Although once considered a low metastatic risk, chordomas have demonstrated distant metastasis to lung, liver, bone, and lymph nodes in up to 48% of patients [5,7,8].

Current treatment is surgery followed by postoperative ionizing radiation (IR). However, in clival chordomas, there seldom is a clean margin due to inaccessibility and proximity to crucial nerve structures [9]. While initial response rates can be good, the tumors are radiation resistant [1,10], are dose limited by surrounding tissue tolerance [1,11], and often recur or metastasize [10,12]. After surgical resection, chordoma recurs in up to 50% of patients [13] and metastasizes in up to 48% of patients [5,7,8]. There are currently no targeted therapies and no chemotherapies for chordoma. Five- and 10-year survival rates are suggested to vary between 70% and 80% and between 30% and 40%, respectively [5,14].

The population of chordoma cells in tissue culture is aggressive yet slow growing and contains cohesive clusters as well as those growing as monolayers [9]. Since cell adhesion can be protective in epithelial tumor cell populations [15], we characterized the epithelial adhesion characteristics of the chordoma population and determined if DNA damage responses (DDRs) were uniform across the population. The cohesive cluster phenotype facilitates metastasis and can offer greater radiation resistance than single cells or strands of cells [15] due to cell-adhesion mediation, including the expression of cytokeratin 8 and 18 in tumor cell clusters. Previous work demonstrated that $\beta 1$ integrins are a determining factor in radiation resistance [12,16], occurring via blockage of $\beta 1$ integrin function or the associated downstream signaling via focal adhesion kinase and integrin-linked kinase [17]. Identifying whether laminin-binding $\beta 1$ integrins ($\alpha 3\beta 1$, $\alpha 6\beta 1$) are involved in IR responses can allow targeting of specific molecular pathways to inhibit the DDR and increase IR effectiveness. In the current study, the DDR of human U-CH1 chordoma cells to IR was determined in both the individual cells and cells within clusters.

An integrin ligand mimetic, HYD1, which can prevent cluster formation, and AIIB2, a function-blocking $\beta 1$ integrin-specific antibody, were tested to determine effects on IR response and survival. The DDR was estimated by the time-dependent detection of four indicators of DDR (γ H2AX, pKAP1, pATM) in the U-CH1 cells. If chordoma cohesive clusters have a muted DDR to IR as compared to the coexisting single-cell monolayer, then targeting the integrin-mediated adhesion complex may increase the effectiveness of IR and perhaps reduce recurrence. Chordomas are homogenous in the cell-cell expression of $\alpha 6$ integrin (this study), and understanding the increased DDR via laminin-binding integrins (LBI) will offer insight into the treatment of other slow-growing epithelial tumors treated with IR, especially the mechanism of cell adhesion-mediated radiation resistance in subtypes of breast and prostate cancer.

Materials and Methods

Cells and IR Treatment

The human U-CH1 cells (ATCC, CRL-3217) originated from a recurrent sacral chordoma after initial radiation therapy and contain several genomic copy number alterations [18]. U-CH1 has a heterogeneous morphology consisting of physaliferous cells with a mucinous intercellular substance that represents typical chordoma features. The UM-CHOR1 cell line (ATCC, CRL-3270) is representative of clival, chondroid-type tumors. Both cell lines overexpress the transcription factor T (brachyury) that is the most specific marker for chordoma. The cells were maintained in Iscove's DMEM:RPMI medium, 4:1 (Mediatech, Inc., Manassas, VA) supplemented with 10% (v/v) fetal bovine serum (FBS) (Peak Serum, Fort Collins, CO) and 1% (w/v) L-glutamine (Life Technologies, Grand Island, NY). DU145 prostate cancer cell line (ATCC, HTB-81) and PrEC, a normal prostate cell line [19], were cultured in Iscove's modified Dulbecco's medium supplemented with 10% FBS. All of the cell lines were cultured at 37°C in a 95% air and 5% CO₂ atmosphere at constant humidity. Cell line identity was validated using short tandem repeat analysis by the Human Origins Genotyping Laboratory at the University of Arizona. The 8-Gy dose was chosen as it represents the total dose (2-Gy fractions \times 4 fractions) that is clinically relevant for chordoma. Cells were irradiated using ⁶⁰Co fixed γ radiation source with a dose rate of 0.62 Gy/min.

Antibodies and Reagents

Antibodies used for immunofluorescence staining include: anti- $\alpha 6$ integrin J1B5 (rat monoclonal, <http://dshb.biology.uiowa.edu/>), anti- $\alpha 3$ integrin P1B5 (mouse monoclonal, EMD Millipore, Billerica, MA), anti-cytokeratin 8/18 (mouse monoclonal 10.11, Dr. Raymond B. Nagle, University of Arizona), anti-PML (mouse monoclonal PG-M3, Santa Cruz Biotechnology, Dallas, TX), and anti-H2AX phospho-serine139 (rabbit monoclonal 20E3, Cell Signaling Technologies, Danvers, MA). F-actin was detected using Alexa Fluor 488 Phalloidin, and nuclear DNA staining was detected with NucBlue Fixed Cell Stain (Life Technologies, Grand Island, NY). The anti- $\alpha 6$ antibody AA6NT (rabbit) [20] was used for tissue staining. Antibodies used for flow cytometry include: Brachyury (goat polyclonal, R&D Systems AF2085, Minneapolis, MN), YAP (rabbit monoclonal D8H1X, Cell Signaling Technology), anti- $\alpha 6$ integrin CD49f PE conjugated (rat monoclonal GoH3, eBioscience, San Diego, CA), anti- $\alpha 3$ integrin CD49c APC conjugated (mouse monoclonal P1B5, eBioscience), anti- $\beta 1$ integrin CD29 PE conjugated (mouse monoclonal TS2/16, BioLegend, San Diego, CA), anti- $\beta 4$ integrin CD104 eFluor660 conjugated (rat monoclonal 439-9B, eBioscience), CD44 (mouse monoclonal 156-3C11, Cell Signaling Technology), anti-H2AX phospho-serine 139 Alexa Fluor 488 conjugated (mouse monoclonal 2F3, BioLegend), anti-KAP1 phospho-serine 824 (rabbit polyclonal, Bethyl A300-767A, Montgomery, TX), and anti-ATM phospho-serine 1981 PE conjugated (mouse monoclonal 10H11.E12, BioLegend). The DNA marker 7-AAD (BioLegend) was used to analyze the cells based on their G1/G2 phase. Laminin mimetic peptide (HYD1) was used as previously reported [21]. $\beta 1$ integrin (CD29) rat antibody (AIIB2) hybridoma, specific for amino acids 207 to 218, was obtained from the University of Iowa (<http://dshb.biology.uiowa.edu/>) and used under azide-free conditions.

Tissue Staining and Immunofluorescence Microscopy

Informed patient consent and Institutional Review Board approval for tissue collection were done through St. Joseph's Hospital and Medical Center. Formalin-fixed deidentified human cancer tissue sections were provided by the Biobank Core Facility at St. Joseph's Hospital and Medical Center and the Barrow Neurological Institute; tissue samples were stained using a Discovery XT Automated Immunostainer (Ventana Medical Systems, Inc., Tucson, AZ) in the TACMASR core support service within the UA Cancer Center. Samples were imaged using an Olympus BX40 system (Southwest Precision Instruments, Tucson, AZ, USA) with a 4× (NA 0.13) and 40× objective (NA 0.75).

U-CH1 cells were grown to 70% confluence on glass coverslips coated with 0.1% (v/v) gelatin (ATCC, PCS-999-027) and were fixed with 3.7% (v/v) neutral buffered formalin for 30 minutes at room temperature and permeabilized for 10 minutes with PBS containing 0.1% (v/v) BSA and 0.2% (v/v) Triton X-100. Cells were incubated with antibodies for 30 minutes in PBS containing 0.1% (v/v) BSA. Coverslips were mounted on slides using Prolong Diamond antifade (Life Technologies). Images were acquired using the Zeiss Axiophot Microscope equipped with a cooled charge-coupled device camera (CoolSNAP HQ2; Photometrics). The scoring of two or more foci was used as a measure of a positive signal in line with published work [22,23].

Flow Cytometry Analysis

Flow cytometry analysis was used to quantitate a variety of cell surface proteins (integrins $\alpha 6$, $\alpha 3$, $\beta 1$, $\beta 4$, and CD44) expressed on U-CH1 cells grown on 0.1% (v/v) gelatin-coated tissue culture flasks. The tumor cells were harvested using 0.1% Trypsin-EDTA (Life Technologies), resuspended in their culture media, and then centrifuged at 1000 rpm at 4°C. The cells were fixed with 2% paraformaldehyde for 20 minutes at room temperature. They were then resuspended in PBS containing 0.2% BSA and allowed to incubate at room temperature for 15 minutes. They were then recentrifuged and resuspended in 200 μ l of PBS containing 0.2% BSA and the appropriate concentration for each of the cell surface protein antibodies. To quantitate the DDR markers (γ H2AX, pKAP1, p-ATM) or transcription factors (Brachyury and YAP), the cells were harvested in the same manner and then fixed, permeabilized, and stained according to the manufacturer's instructions using the BioLegend Nuclear Factor Fixation/Permeabilization Kit. Approximately 1.0 to 2.0×10^6 cells were used per experimental condition. The cells were analyzed on a BD Accuri C6 Plus instrument (BD Biosciences, San Jose, CA), and the data were analyzed using FlowJo Data Analysis Software v10 (FlowJo, LLC). To account for differences in cell cycle distribution that affect average DDR signal intensity measurements under all experimental conditions, specific DDR end point expression was shown as a function of DNA content. The results were expressed as a ratio of the signal intensity for positive DDR expression and total DDR expression in cells containing a G1 DNA content.

Cytotoxicity Assay

MTT dye metabolism was used to assay cell viability as previously described [24]. To determine cytotoxicity of IR treatment, cells were seeded in 96-well plates; incubated for 24 hours; irradiated; grown for 7, 14, or 28 days; and processed for viability. While radiation sensitivity with clonogenic survival has remained the investigation of

choice since 1955 [25], the MTT assay is an established method of radiation sensitivity when cells, such as chordoma, will not clone into a colony for counting. A minimum of four cell doubling times (in this case, 28 days) is required to assess radiation sensitivity [26]. U-CH1 cells have a doubling time of up to 7 days [18,27]. To assess viability, cells were incubated in culture media for 4 hours with PBS containing MTT dye, the solution was removed, and the resulting purple formazan product was solubilized in DMSO. The quantification of the product was achieved using absorbance measurements at 540 nm using a μ Quant microplate reader (BIO-TEK, Winooski, VT). The survival curves were generated by sigmoidal analysis of the dose response data using GraphPad Prism v5.0c software (GraphPad, La Jolla, CA).

Statistical Analysis

Differences in means between groups were evaluated by two-tailed test of population proportion or two-tailed Student's *t* tests performed in Origin v6.1 software (Northampton, MA) and GraphPad Prism v5.0c software (GraphPad, La Jolla, CA), respectively. For all of the analyses, statistical significance was assigned at *P* value $\leq .05$. Unless otherwise stated, all data are presented as mean \pm SD.

Results

Chordoma Mixed Epithelial Phenotype of 2D Spread Cells and 3D Cohesive Clusters

Previous work has shown a heterogeneous population of chordoma tumor cells containing cells growing as a monolayer and within clusters, identified both by transmission electron microscopy and by bright field microscopy [28]. The chordoma cells express $\alpha 6$ integrin (CD49f), one of the laminin-binding integrins and a stem cell marker in many epithelial types, including nucleus pulposus stem cells of the primitive notochord from which chordomas are derived [3,6]. The 2D chordoma cells growing in a single cell monolayer expressed an extensive cytokeratin 8 and 18 filamentous network and F-actin (Figure 1A). The cytokeratin filament networks were cytoplasmic, did not colocalize with F-actin, and wrapped around the cell nucleus as expected for intact epithelial intermediate filaments. Other cytokeratin filaments (e.g., cytokeratin 5 and 14, specific for basal cells; cytokeratin 6, specific for hyperproliferative cells; and cytokeratin 1 and 10, specific for epithelial cells) were undetectable, indicating that the cytokeratin networks observed were similar to other epithelial tumors and not lineage specific (Supplemental Table S1).

The $\alpha 6$ integrin was observed primarily in the cytoplasm (Figure 1B). Within the same culture, 3D cohesive clusters of tumor cells retained expression of $\alpha 6$ integrin and F-actin in a reorganized distribution (Figure 1C) with abundant cell-cell surface expression of the integrin and F-actin in a cortical-like distribution. Tissues from archived specimens of 42 resections of human chordoma, representing 23 different chordoma patients (deidentified), were stained with $\alpha 6$ integrin-specific antibody. The distribution of $\alpha 6$ integrin was on the tumor cell surface within single cell-type populations (Figure 1D) and within cell clusters in a cell-cell distribution (Figure 1E). The integrin staining in tissue sections was abundant and in a distribution consistent with the known foamy and physaliferous pattern seen in chordoma (Supplemental Figure S1). Approximately 15% of the U-CH1 chordoma population was contained in 3D clusters, which was significantly decreased by providing the HYD1 ligand mimetic (Figure 1F). The total cell population, independent of cluster

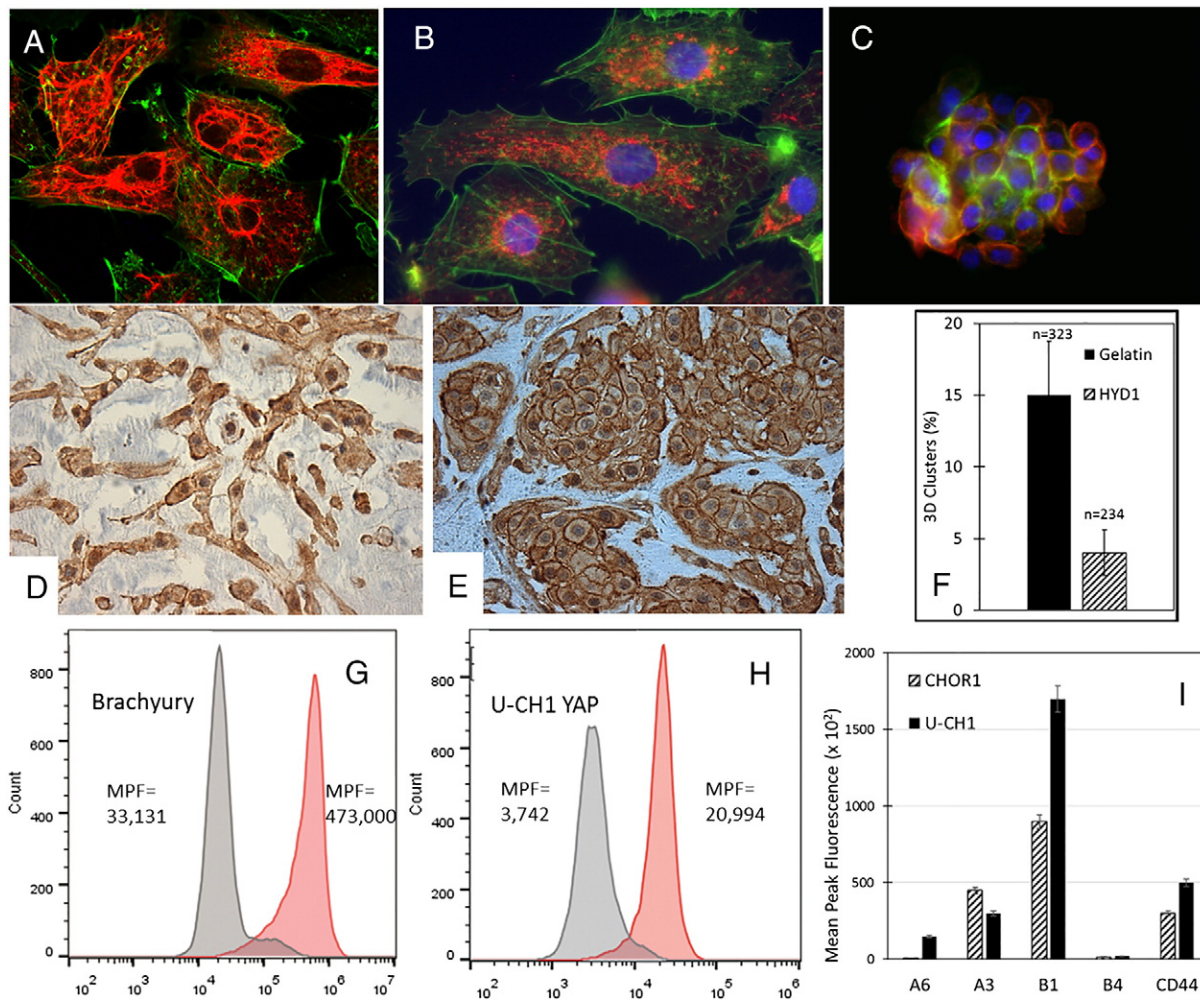


Figure 1. Chordoma epithelial characteristics in single cells and clusters. Human chordoma tissue (42 resections, 23 patients). (A) U-CH1 single cells, F-actin (green), and cytokeratin 8 and 18 (red) expression. (B) U-CH1 single cells containing actin (green), $\alpha 6$ integrin (red), and DNA (blue). (C) U-CH1 clusters containing actin (green), $\alpha 6$ integrin (red), and nuclear DNA (blue). (D and E) Human chordoma specimen stained for $\alpha 6$ integrin (brown). (F) The percentage of cells in the population contained within cohesive clusters under normal coating conditions (gelatin) or grown on immobilized HYD1 (HYD1), a laminin ligand mimetic. Flow cytometry profiles of (G) brachyury and (H) YAP. (I) Expression and mean peak fluorescence values for surface expression of $\alpha 6$ integrin (CD49f), $\alpha 3$ integrin (CD49c), $\beta 1$ integrin (CD29), $\beta 4$ integrin (CD104), and MUC1 (CD44) in UCH-1 (solid black) or CHOR1 (striped) cells.

phenotype, expressed brachyury and YAP transcriptional regulators in a uniform distribution as detected by flow cytometry (Figure 1, G and H). The cell surface expression of $\alpha 6$, $\alpha 3$, $\beta 1$, and $\beta 4$ integrins and CD44 (Figure 1I) was analyzed by flow cytometry and quantitated by determining the mean peak fluorescence values for the entire population, whether grown as individual cells or cohesive clusters. Both U-CH1 and CHOR1 cells showed a uniform population distribution of all five adhesion receptors from which the mean peak values were derived.

Heterogenous DDR in Chordoma Population

Since chordoma is treated with a combination of surgery and radiation therapy, we determined the DDR of the U-CH1 chordoma population to radiation. We used three well-studied DDRs to IR: γ H2AX (p-serine 139), pKAP1 (p-serine 824), and pATM (p-1981) analyzed by flow cytometry [29]. Normal prostate (PrEC) and tumor (DU145) epithelial cells were used for comparison purposes to chordoma (U-CH1). Prostate cell lines were used for comparison to

chordoma since both share the same epithelial characteristics and are slow growing, IR resistant, and treated clinically with IR.

In chordoma cell cells, a nonresponsive population (approximately 50%) was documented in both the γ H2AX and the pKAP1 DDR profiles in response to 8 Gy (Figure 2). The γ H2AX response analysis was restricted to the G1 population to avoid the known constitutive signaling within the G2 population [30]. The data showed that while the majority of the DU-145 cells were positive for both DDR endpoints, a significant population of the chordoma cells was defective. It is interesting to note that the nonresponsive population in the chordoma cells occurred independent of the cell cycle distribution.

The Cohesive Cluster Phenotype and a Muted IR-Induced γ H2AX Signal

We utilized the F-actin stain to locate 3D cohesive cell clusters distinct from 2D cells within the population and confirmed their location by the cluster of nuclei detected by a DNA stain (DAPI).

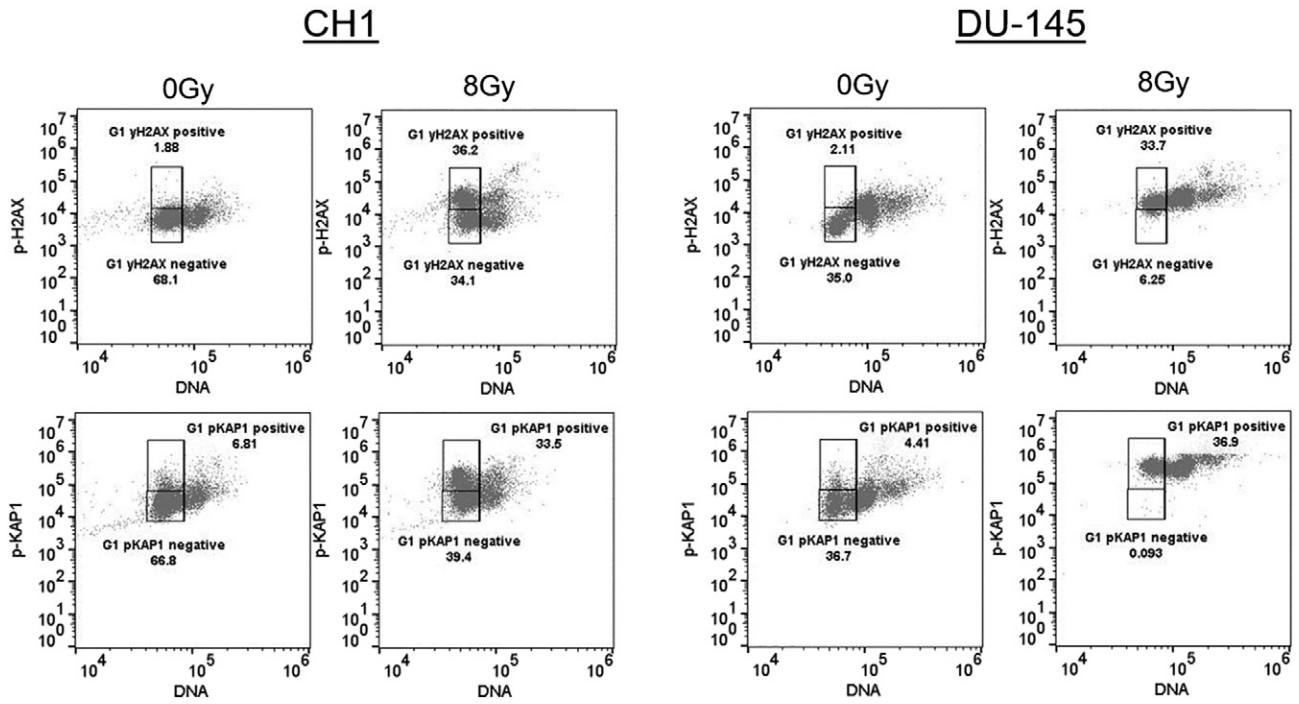


Figure 2. Quantification of the DDR to IR in cell populations by flow cytometry. Chordoma (CH1) and prostate cancer (DU-145) cells were either untreated (0 Gy) or treated with IR (8 Gy) and tested 1 hour following IR for expression of p-H2AX (top panels) or p-KAP1 (bottom panels) and DNA content in the population (DNA) (all panels). The boxes represent positive and negative gates for the DDR response as a function of G1 DNA content. The numbers represent the % of total events that occur within the positive or negative gates.

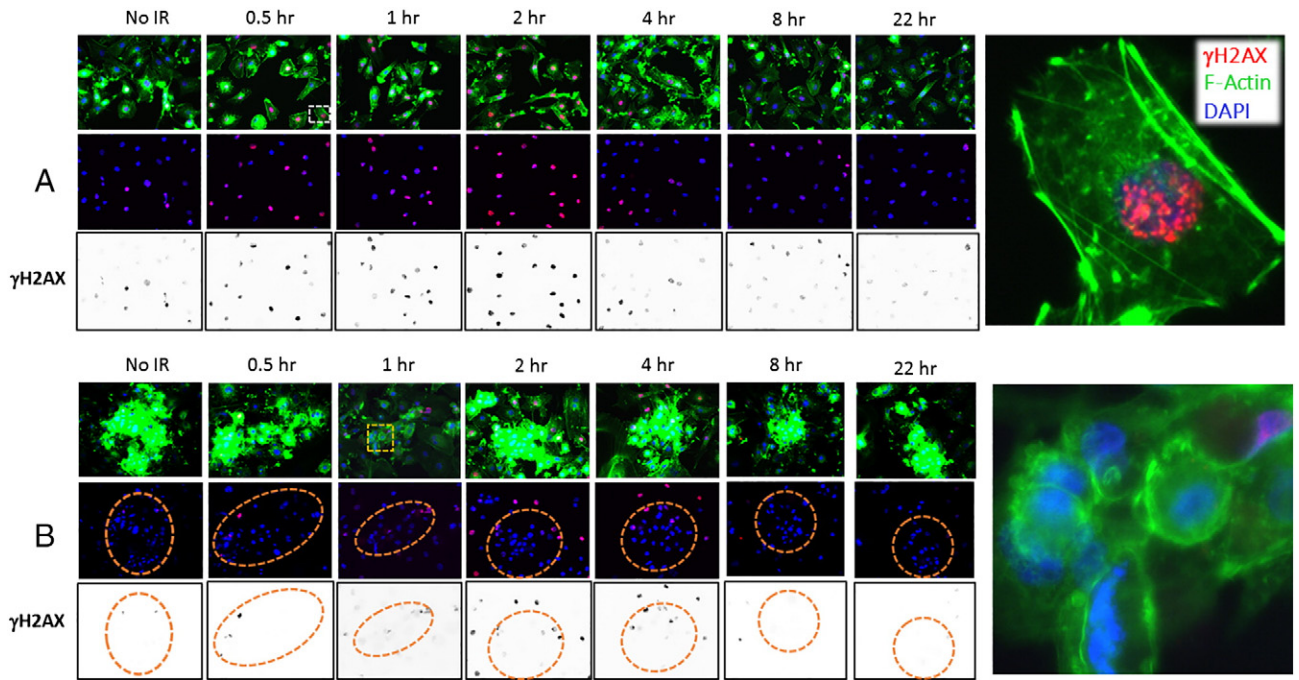


Figure 3. Chordoma cell population contained a heterogeneous DDR to 8-Gy IR. (A) The 2D well-spread chordoma cells stained for F-actin (green), γ H2AX (p-serine 139, red), or nuclear DNA (blue) either without radiation treatment (no IR) or for times up to 22 hours (0.5 to 22 hours) following 8-Gy treatment. Black and white panels represent the γ H2AX channel, converted to greyscale and inverted. (B) The 3D chordoma clusters stained for F-actin (green), γ H2AX (p-serine 139, red), or DNA (blue) either without radiation treatment (no IR) or for times up to 22 hours (0.5 to 22 hours) following 8-Gy treatment. Black and white panels represent the γ H2AX channel, converted to greyscale and inverted. Orange circles mark the chordoma clusters, identified by the F-actin stain (green) and verified by the clusters of nuclei (blue).

Immunofluorescence analysis of the DDR to 8 Gy showed a maximum nuclear signal at approximately 2 hours after the IR treatment that dissipated by 4 hours (Figure 3A). The nuclear γ H2AX signal was scored positive if there were two or more foci within the nuclei (as shown in the representative image in Figure 3A). An immunofluorescence analysis of the cohesive clusters (Figure 3B) showed a significantly reduced nuclear signal at approximately 2 hours after IR as compared to the 2D cells (Supplemental Figure S2). Using the F-actin staining to detect the cell-cell clusters, we quantified the percentage of γ H2AX-positive cells in response to IR in the 2D and 3D clusters.

In the 2D population, approximately 25% of the cells were positive for nuclear γ H2AX foci in the absence of IR (Figure 4). Approximately twice as many cells had a significant increase in the γ H2AX signal within a 30-minute repair interval, which continued to increase with an estimated 75% of cells responding by 2 hours. The signal 4 hours after the IR dose was not significantly different than the unirradiated sample, consistent with a resolution of the DDR. Within 8 hours of the IR treatment, approximately 60% of the 2D cells contained an increase in the γ H2AX signal, which was expected to occur in part from the known IR-induced G2 progression block; within 22 hours after IR, the γ H2AX signal was not significantly different as compared to unirradiated cells.

In the 3D cluster chordoma population, approximately 2% of the cells were positive for nuclear γ H2AX foci in the absence of IR (Figure 4) as compared to 25% of the population within the 2D cells. There was no significant increase in the γ H2AX signal within a 30-minute repair interval. However, approximately 15% of the cells within the 3D clusters responded by 2 hours as compared to the unirradiated 3D clusters. Within 4 hours after the IR dose, the signal in the 3D clusters remained significantly different from the unirradiated 3D sample. Within 8 and 22 hours of the IR treatment, the 3D clusters contained levels not significantly different than of the unirradiated 3D clusters.

Taken together, the results show that the 2D spread cells and the 3D cohesive clusters, while coexisting in the same population, have a significantly different γ H2AX DDR. In particular, whereas 75% of the 2D cells will respond (Figure 4), only 15% of the cells in the 3D cluster will contain the expected γ H2AX DDR (Figure 4). During the repair interval, the 2D cells resolved the γ H2AX foci within 4

hours. In comparison, the cells within the 3D cluster still contained γ H2AX foci at 4 hours of repair that were significantly elevated in relation to the unirradiated 3D cells (Figure 4). These results indicate that the 3D clustered cells—as compared to the 2D cells—have a significantly reduced γ H2AX response to 8-Gy IR treatment and that the damage response that does exist requires more time to resolve.

The Time and Dose Dependence of the Chordoma DDR is Defective

Since the γ H2AX signal is a DDR sensor that is a modification of the histone component of chromatin [31], we next investigated the pKAP1 (p-serine 824) response, another IR-dependent chromatin modifying event [29]. Monitoring the time response following 8-Gy IR in the G1 population showed that the chordoma cells contained only a maximum of 50% of the cells responding with either the γ H2AX or the pKAP1 signal (Figure 5, top panels). The pATM signal was not observed in the chordoma cells at any time or any dose tested as compared to a response seen in the normal PrEC cells (Figure 5, far right panels). The γ H2AX dose response to IR in DU145 cells was verified by comparing the flow data with the Western blot and the immunofluorescence microscopy (Supplemental Figure S3).

Peptide Ligand Mimetic Delays γ H2AX Resolution and Sensitizes to IR Cell Killing

Since the U-CH1 3D clusters contained LBI (Figure 1) and the U-CH1 3D clusters are nonresponsive to IR-induced DDR signals (Figs. 2-5), we next tested the ability of a peptide ligand mimetic of the laminin-binding integrins, HYD1, to alter the γ H2AX DDR response in U-CH1 cells. HYD1 was used to provide a synthetic surface that can promote adhesion uncoupled from integrin downstream signaling [32]. HYD1 decreased the percentage of cells growing as 3D clusters to less than 5% of the population (Figure 1F). The γ H2AX response was monitored by immunofluorescence in unirradiated (no IR) cells or 2 or 24 hours after 8 Gy IR (Figure 6A). Approximately 70% of the U-CH1 cells were positive for the γ H2AX signal 2 hours following 8-Gy IR, independent of the HYD1 treatment (Figure 6A). However, the presence of HYD1 significantly reduced the resolution of the DDR response since twice as many cells had microscopy of the resulting 2D U-CH1 cells. The DDR of the 2D cells was scored and retained the γ H2AX signal at 24 hours after

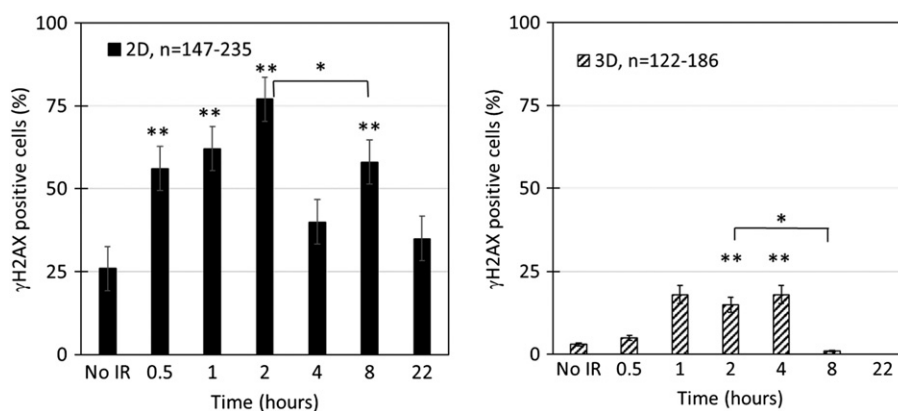


Figure 4. Muted DDR in cohesive chordoma clusters as compared to well-spread 2D cells. Quantitation of the percentage of nuclei containing γ H2AX foci in 2D cells (A) or 3D cells (B) following 8-Gy IR. Statistical significance assessed by two independent proportions test. ** $P < .005$, as compared to no IR; * $P < .005$, comparing bracketed pair.

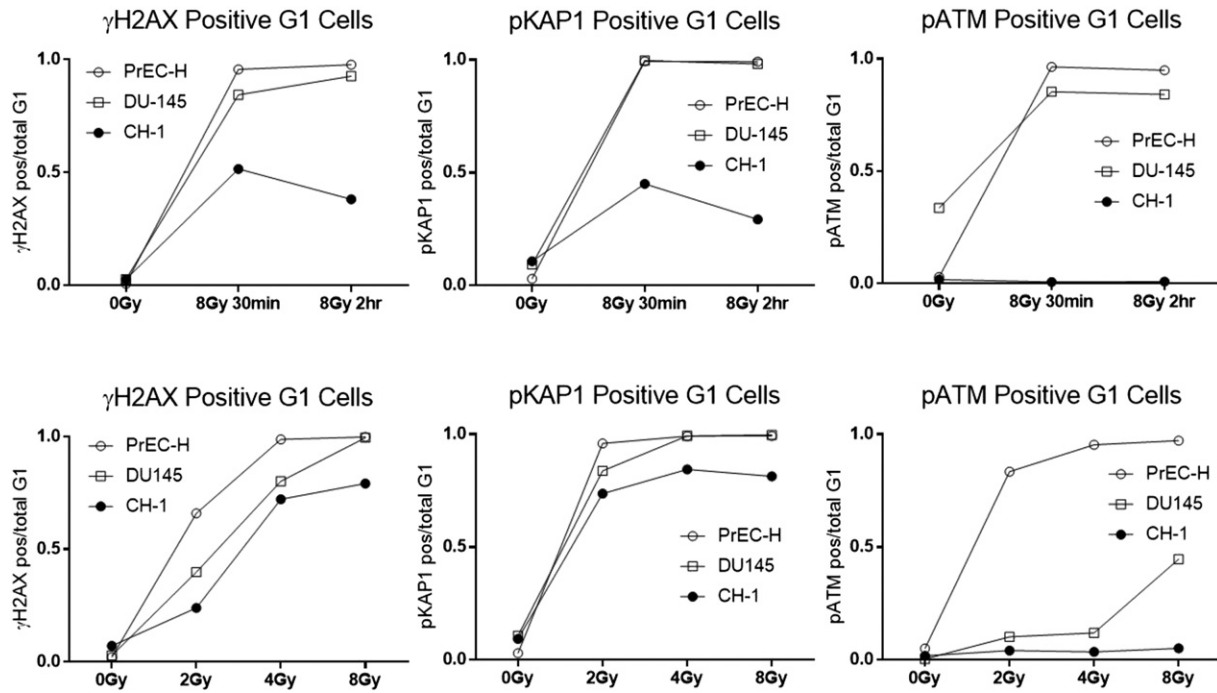


Figure 5. Time and dose dependence of the DDR to IR in G1 cell populations. Normal prostate epithelial cells (PrEC-H), prostate cancer (DU145) cells, or chordoma (UCH-1) cells were either untreated (0 Gy) or treated with IR (8 Gy) and tested 30 minutes or 2 hours following IR for expression of p-H2AX (top left panels), pKAP1 (top middle panels), or pATM (top right panels). The DDR response was also determined following increasing doses of IR at 1 hour after treatment (bottom panels). The ratio of the positive events to the total events within the G1 DNA content gates is shown.

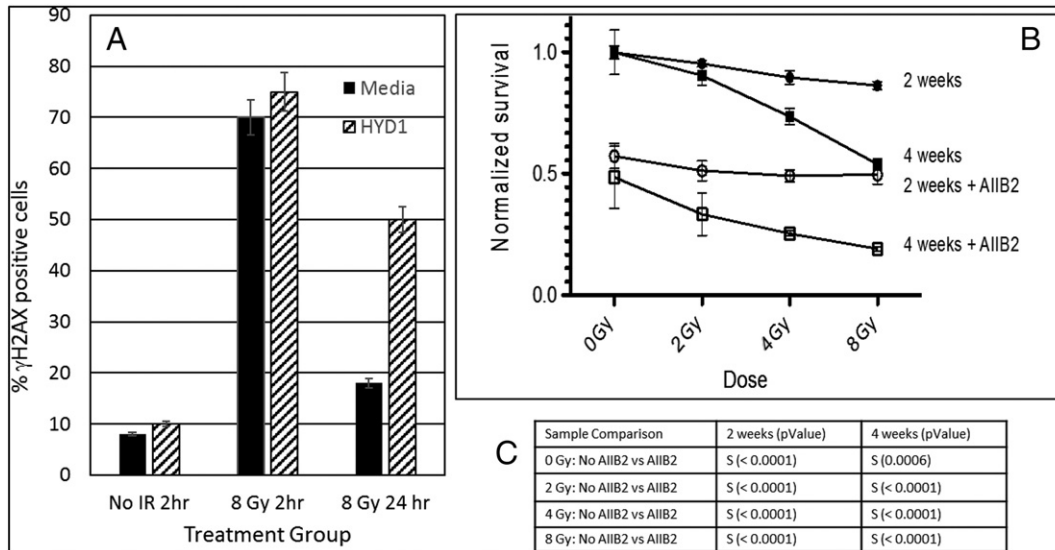


Figure 6. Laminin ligand mimetic prevents resolution of the DDR response in 2D well-spread chordoma cells, and integrin-blocking antibody sensitizes cells to the lethal effects of IR. (A) U-CH1 cells were either untreated (media) or grown on laminin ligand mimetic (1 μ g/ml of HYD1) for 24 hours prior to exposure to 8-Gy IR. The γ H2AX response was monitored in 2D well-spread cells by IFM analysis (% positive cells) after 2 or 24 hours following radiation treatment (8 Gy) or in unirradiated samples (no IR). At least 150 cells were counted in each group, and the errors are 2 SDs above the mean. (B) MTT survival curve of U-CH1 cells either unirradiated (0 Gy) or exposed to different doses (2, 4, 8 Gy) of IR either with (open symbols) or without (closed symbols) β 1 integrin blocking antibody after 2 (circles) or 4 (squares) weeks of growth. The percent survival is determined by the change in the OD reading of the MTT dye as compared to untreated cells. Symbols represent mean \pm SD. (C) Student's *t* test was used to determine significant difference (S) = *P* < .0001 in the sample comparison groups listed at both 2 and 4 weeks.

8-Gy IR as compared to the untreated group (Figure 6A). Since retention of the γ H2AX signal can indicate unrepaired double-stranded DNA breaks [33] and one double-stranded DNA break can be lethal [34], we tested the ability of a β 1 integrin-blocking antibody called AIIB2 to increase the lethal effects of IR in the U-CH1 cell population. U-CH1 cells were exposed to different doses of IR either with or without AIIB2. The U-CH1 cells were tested for viability using the MTT assay at 2 and 4 weeks after the irradiation to be certain that any lethal effects due to potentially lethal damage repair would be detected. As a single agent, the AIIB2 had a striking effect on U-CH1 cell survival as the surviving fraction was approximately 50% at both 2 and 4 weeks. Combining the AIIB2 with different doses of IR showed approximately a doubling of the cell killing at all the doses tested.

Discussion

Three different endpoints (γ H2AX, pKAP1, and pATM) of DDR were analyzed in a rare but lethal epithelial-type tumor (chordoma) and compared to normal and adenocarcinoma cells. In normal epithelial cells, an increasing DDR response (γ H2AX, pKAP1) was observed 1 hour following increasing doses of IR (2, 4, 8 Gy). All three DDRs were maximal at 2.0 hours following the DNA damage and resolved to baseline levels within 3 hours after IR. A remarkable finding was that a subpopulation of U-CH1 cells did not respond to IR doses with a γ H2AX or pKAP1 signal. In the case of pATM, the chordoma U-CH1 line, derived from recurrent disease after IR therapy [18], was uniformly not responsive and may be in line with recent reports that pATM defects portend recurrent epithelial tumors [35].

Approximately 15% of the U-CH1 cells were designated as a “nonresponder” subpopulation to both γ H2AX and pKAP1 and were observed growing as cohesive clusters. By supplying HYD1, a d-amino acid-containing peptide that acts as a ligand mimetic to drive adhesion while uncoupling integrin-dependent signaling [32], production of these cohesive clusters decreased to less than 5% of the population. This corresponded to a significant increase in the responding γ H2AX and pKAP1 populations and a delay in the resolution of the γ H2AX signal during the repair interval. The delay in γ H2AX foci resolution indicates a defect in repair [36]. Using the HYD1 peptide to decrease the cohesive cluster phenotype may be a method to increase the sensitivity of chordoma to DNA-damaging agents. The β 1 integrin-blocking antibody (AIIB2) was striking in its ability to decrease chordoma cell survival as a single agent. The ability of AIIB2 to induce cell death in the absence of IR may be related to the known induction of programmed cell death originally described in normal cells with the loss of cell-ECM adhesion [37]—if this were the case, then protein kinase signaling pathways could be targeted as well. AIIB2 treatment also significantly increased the lethal effects of IR. Taken together, these results suggest that phenotypic changes induced by the ECM can influence the DDR response. This is indicative that phenotypic targeting may be an effective strategy to increase the lethality of known anticancer agents [35]. We note with interest that systemic agents are currently being tested to inactivate β 1 integrin function in tumors [38,39]. Future formulations of HYD1, as a ligand mimetic, may offer a potential local therapy approach.

During the course of these studies, a major question arose as to whether the cohesive phenotype represents a distinct subpopulation of cells or represents an inducible phenotype within the population. While the cohesive clusters can be retrieved physically from the

population, they readily form into the 2D well-spread phenotype and result in a mixed population. Similarly, specific isolation of the 2D well-spread cells will recapitulate the mixed population. The mixed phenotype of the population appears to be a characteristic of the cell line, perhaps reflecting its stem cell-like properties and origin [18]. Current interest in the tumor ecosystem [40] may uncover mechanisms by which surrounding tissue, including adipocytes and their associated immune cells, influences the development and phenotype of the tumor cells. It may be that future experiments to induce differentiation of chordoma-type tumors could be a strategy for making the tumor self-limiting.

The use of HYD1 as a ligand mimetic was striking in its ability to decrease the cell-cell cohesive clusters, promote the cell-ECM attached cell phenotype in chordoma, and decrease the resolution of γ H2AX foci. We note that HYD1 can uncouple adhesion and integrin signaling functions, [32] and in this study, it decreased the cell-cell structural phenotype of the chordoma cell line. It remains to be determined if the cell-cell structural phenotype in chordoma is the critical element of IR resistance or if conversion to 2D adherent phenotype could be exploited for anti- β 1 integrin therapeutics. In either case, acknowledging and investigating the heterogeneity of the DDR response in chordoma could provide new approaches to its eradication. The mixture of adhesion phenotypes and DDR observed here suggests that a combination strategy of targeting cell-ECM and cell-cell adhesion properties would be effective in chordoma *in vivo*. Future studies utilizing patient-derived xenografts could offer an approach to test this hypothesis.

Acknowledgements

University of Arizona Cancer Center Radiation Core Facility was used to irradiate the tissue culture samples. Deidentified patient tissue samples obtained with informed consent and Institutional Review Board approval were provided by the Biobank Core Facility at St. Joseph's Hospital and Medical Center and the Barrow Neurological Institute.

Appendix A. Supplementary Data

Supplementary data to this article can be found online at <https://doi.org/10.1016/j.neo.2017.08.005>.

References

- Walcott BP, Nahed BV, Mohyeldin A, Coumans JV, Kahle KT, and Ferreira MJ (2012). Chordoma: current concepts, management, and future directions. *Lancet Oncol* **13**, e69–e76.
- Catton C, O'Sullivan B, Bell R, Laperriere N, Cummings B, Fornasier V, and Wunder J (1996). Chordoma: long-term follow-up after radical photon irradiation. *Radiother Oncol* **41**, 67–72.
- Shen J, Shi Q, Lu J, Wang D, Zou T, Yang H, and Zhu G (2013). Histological study of chordoma origin from fetal notochordal cell rests. *Spine* **38**, 2165–2170.
- Scheil-Bertram S, Kappler R, von Baer A, Hartwig E, Sarkar M, Serra M, Bruderlein S, Westhoff B, Melzner I, and Bassaly B, et al (2014). Molecular profiling of chordoma. *Int J Oncol* **44**, 1041–1055.
- Chugh R, Tawbi H, Lucas DR, Biermann JS, Schuetz SM, and Baker LH (2007). Chordoma: the nonsarcoma primary bone tumor. *Oncologist* **12**, 1344–1350.
- George B, Bresson D, Herman P, and Froelich S (2015). Chordomas: a review. *Neurosurg Clin N Am* **26**, 437–452.
- Young VA, Curtis KM, Temple HT, Eismont FJ, DeLaney TF, and Hornicek FJ (2015). Characteristics and patterns of metastatic disease from chordoma. *Sarcoma* **20**, 1–7.

- [8] Rohatgi S, Ramaiya NH, Jagannathan JP, Howard SA, Shinagare AB, and Krajewski KM (2015). Metastatic chordoma: report of the two cases and review of the literature. *Eur J Med* **47**, 151–154.
- [9] Yadav R, Sharma MC, Malgulwar PB, Pathak P, Sigamani E, Suri V, Sarkar C, Kumar A, Singh M, and Sharma BS, et al (2014). Prognostic value of MIB-1, p53, epidermal growth factor receptor, and INI1 in childhood chordomas. *Neuro Oncol* **16**, 372–381.
- [10] Fernandez-Miranda JC, Gardner PA, Snyderman CH, Devaney KO, Mendenhall WM, Suarez C, Rinaldo A, and Ferlito A (2014). Clival chordomas: a pathological, surgical, and radiotherapeutic review. *Head Neck* **36**, 892–906.
- [11] Bjornsson J, Wold LE, Ebersold MJ, and Laws ER (1993). Chordoma of the mobile spine. a clinicopathologic analysis of 40 patients. *Cancer* **71**, 735–740.
- [12] Eke I, Deuse Y, Hehlhans S, Gurtner K, Krause M, Baumann M, Shevchenko A, Sandfort V, and Cordes N (2012). $\beta(1)$ Integrin/FAK/cortactin signaling is essential for human head and neck cancer resistance to radiotherapy. *J Clin Invest* **122**, 1529–1540.
- [13] von Witzleben A, Goertler L, Lennerz J, Weissinger S, Kornmann M, Mayer-Steinacker R, von Baer A, Schultheiss M, Möller P, and Barth TE (2015). In chordoma, metastasis, recurrences, Ki-67 index, and a matrix-poor phenotype are associated with patients' shorter overall survival. *Eur Spine J*, 1–9.
- [14] Horbinski C, Oakley GJ, Ciepły K, Mantha GS, Nikiforova MN, Dacic S, and Seethala RR (2010). The prognostic value of Ki-67, p53, epidermal growth factor receptor, 1p36, 9p21, 10q23, and 17p13 in skull base chordomas. *Arch Pathol Lab Med* **134**, 1170–1176.
- [15] Harryman WL, Hinton JP, Rubenstein CP, Singh P, Nagle RB, Parker SJ, Knudsen BS, and Cress AE (2016). The cohesive metastasis phenotype in human prostate cancer. *Biochim Biophys Acta* **1866**, 221–231.
- [16] Jahangiri A, Aghi MK, and Carbonell WS (2014). $\beta 1$ Integrin: critical path to antiangiogenic therapy resistance and beyond. *Cancer Res* **74**, 3–7.
- [17] Hoshino A, Costa-Silva B, Shen T-L, Rodrigues G, Hashimoto A, Tesic Mark M, Molina H, Kohsaka S, Di Giannatale A, and Ceder S, et al (2015). Tumour exosome integrins determine organotropic metastasis. *Nature* **527**, 329–335.
- [18] Scheil S, Bruderlein S, Liehr T, Starke H, Herms J, Schulte M, and Moller P (2001). Genome-wide analysis of sixteen chordomas by comparative genomic hybridization and cytogenetics of the first human chordoma cell line, U-CH1. *Genes Chromosomes Cancer* **32**, 203–211.
- [19] Garraway LA, Lin D, Signoretti S, Waltregny D, Dilks J, Bhattacharya N, and Loda M (2003). Intermediate basal cells of the prostate: in vitro and in vivo characterization. *Prostate* **55**, 206–218.
- [20] Ports MO, Nagle RB, Pond GD, and Cress AE (2009). Extracellular engagement of $\alpha 6$ integrin inhibited urokinase-type plasminogen activator-mediated cleavage and delayed human prostate bone metastasis. *Cancer Res* **69**, 5007–5014.
- [21] Sroka IC, Anderson TA, McDaniel KM, Nagle RB, Gretzer MB, and Cress AE (2010). The laminin binding integrin $\alpha 6 \beta 1$ in prostate cancer perineural invasion. *J Cell Physiol* **224**, 283–288.
- [22] Olive PL and Banath JP (2009). Kinetics of H2AX phosphorylation after exposure to cisplatin. *Cytometry B Clin Cytom* **76**, 79–90.
- [23] Banuelos CA, Banath JP, Kim JY, Aquino-Parsons C, and Olive PL (2009). γ H2AX expression in tumors exposed to cisplatin and fractionated irradiation. *Clin Cancer Res* **15**, 3344–3353.
- [24] Congdon LM, Pourpak A, Escalante AM, Dorr RT, and Landowski TH (2008). Proteasomal inhibition stabilizes topoisomerase II α protein and reverses resistance to the topoisomerase II poison etoposide (AMP-53, 6-ethoxyazonafide). *Biochem Pharmacol* **75**, 883–890.
- [25] Puck TT and Marcus PI (1955). A rapid method for viable cell titration and clone production with hela cells in tissue culture: the use of x-irradiated cells to supply conditioning factors. *Proc Natl Acad Sci U S A* **41**, 432–437.
- [26] Carmichael J, DeGraff WG, Gazdar AF, Minna JD, and Mitchell JB (1987). Evaluation of a tetrazolium-based semiautomated colorimetric assay: assessment of radiosensitivity. *Cancer Res* **47**, 943–946.
- [27] Kato TA, Tsuda A, Uesaka M, Fujimori A, Kamada T, Tsujii H, and Okayasu R (2011). In vitro characterization of cells derived from chordoma cell line U-CH1 following treatment with X-rays, heavy ions and chemotherapeutic drugs. *Radiat Oncol* **6**, 116–116.
- [28] Kolb D, Pritz E, Steinecker-Frohnwieser B, Lohberger B, Deutsch A, Kroneis T, El-Heliebi A, Dohr G, Meditz K, and Wagner K, et al (2014). Extended ultrastructural characterization of chordoma cells: the link to new therapeutic options. *PLoS One* **9**, e114251.
- [29] Liedtke S, Biebrnick S, Radke TF, Stapelkamp D, Coenen C, Zaehres H, Fritz G, and Kogler G (2015). DNA damage response in neonatal and adult stromal cells compared with induced pluripotent stem cells. *Stem Cells Transl Med* **4**, 576–589.
- [30] Dale Rein I, Stokke C, Jalal M, Myklebust JH, Patzke S, and Stokke T (2015). New distinct compartments in the G2 phase of the cell cycle defined by the levels of γ H2AX. *Cell Cycle* **14**, 3261–3269.
- [31] Kinner A, Wu W, Staudt C, and Iliakis G (2008). γ -H2AX in recognition and signaling of DNA double-strand breaks in the context of chromatin. *Nucleic Acids Res* **36**, 5678–5694.
- [32] Sroka TC, Pennington ME, and Cress AE (2006). Synthetic D-amino acid peptide inhibits tumor cell motility on laminin-5. *Carcinogenesis* **27**, 1748–1757.
- [33] Paull TT, Rogakou EP, Yamazaki V, Kirchgessner CU, Gellert M, and Bonner WM (2000). A critical role for histone H2AX in recruitment of repair factors to nuclear foci after DNA damage. *Curr Biol* **10**, 886–895.
- [34] van Gent DC, Hoeijmakers JH, and Kanaar R (2001). Chromosomal stability and the DNA double-stranded break connection. *Nat Rev Genet* **2**, 196–206.
- [35] Sun Y (2015). Translational horizons in the tumor microenvironment: harnessing breakthroughs and targeting cures. *Med Res Rev* **35**, 408–436.
- [36] Podhorecka M, Skladanowski A, and Bozko P (2010). H2AX phosphorylation: its role in DNA damage response and cancer therapy. *J Nucleic Acids* **2010**.
- [37] Frisch SM and Ruoslahti E (1997). Integrins and anoikis. *Curr Opin Cell Biol* **9**, 701–706.
- [38] Campbell MR, Zhang H, Ziaee S, Ruiz-Saenz A, Gulizia N, Oeffinger J, Amin DN, Ahuja D, Moasser MM, and Park CC (2016). Effective treatment of HER2-amplified breast cancer by targeting HER3 and $\beta 1$ integrin. *Breast Cancer Res Treat* **155**, 431–440.
- [39] Carbonell WS, DeLay M, Jahangiri A, Park CC, and Aghi MK (2013). $\beta 1$ integrin targeting potentiates antiangiogenic therapy and inhibits the growth of bevacizumab-resistant glioblastoma. *Cancer Res* **73**, 3145–3154.
- [40] Horning SJ (2017). A new cancer ecosystem. *Science (New York, NY)* **355**, 1103.